THE DEVELOPMENT OF A HIGH-PRECISION STRAPDOWN INERTIAL SYSTEM BASED ON MEDIUM-ACCURACY FIBER-OPTIC GYROSCOPES FOR ROCKET AND SPACE APPLICATIONS

O.Yu. Zlatkin[1], S.V. Oleynik[2], A.V. Chumachenko[3], Yu.A. Kuznetsov[4], V.D. Kozhuhov[5]

Research Production Enterprise Hartron-Arkos, 1, Academica Proscury str., Kharkov, 61070, Ukraine,
E-mail: inf@hartron-arkos.kharkov.ua, phone: +38 (057) 7191783

V.B. Uspensky[6], A.V. Gudzenko[7]

National Technical University «Kharkov Polytechnic Institute», 21, Frunze str., Kharkov, 61002, Ukraine,
E-mail: v_usp@rambler.ru, phone: +38 (057) 7076454

Abstract

Keywords: strapdown inertial system, fiber-optic gyroscopes, magnetic and thermal sensitivity, calibration, satellite

The technology of creating a high-precision strapdown inertial system on the basis of medium-accuracy fiber-optic gyroscopes (FOG) for rocket and space applications is described. The results of studies of the FOG magnetic and thermal sensitivity, the methods of ground and orbital calibration, and the results of mathematical simulation are presented. The characteristics of the inertial system under development are given.

Introduction

Nowadays designers of control systems for launch vehicles and spacecraft are actively searching for the angular rate sensors (ARS), which are an alternative to mechanical gyroscopes. This group of sensors includes optical sensors (laser and fiber-optic gyroscopes), microelectromechanical systems (MEMS), and Coriolis vibratory gyroscopes. The first strapdown inertial navigation systems (SINS) based on laser gyroscopes have shown that in addition to the benefits, such as a short start-up time, resistance to mechanical stress, there are some shortcomings caused by dithering, sensitivity to the external magnetic field, high noise component of measurements, short service life. MEMS-based devices have low dimensions and mass characteristics, low power consumption, wide dynamic range, however they are not accurate enough to be used in high-precision control systems [1].

FOGs are of particular interest to SINS developers as they have a high measurement precision and a relatively small size, weight, power consumption and a short start-up time. They have a longer service life as compared with laser gyroscopes. Coriolis vibratory gyroscopes are competitive with FOGs in accuracy and other technical characteristics.

Currently, the Research and Production Enterprise (RPE) Hartron-Arkos (Kharkov) is developing strapdown inertial systems on the basis of FOGs designed, primarily, for the Ukrainian rocket and space industry. The strapdown inertial system consists of an inertial measurement unit (IMU) and an electronics unit containing a special computer and a secondary power source. The IMU is equipped with FOGs of the Russian Research and Production Enterprise Optolink (Zelenograd). This company produces a wide range of FOGs, from medium to high-end precision, among which are such single-axis FOGs as OIUS-200, OIUS-501, OIUS-1000, OIUS-2000, three-axis FOGs, and an IMU based on FOGs [2, 3].

RPE Hartron-Arkos is developing an IMU based on medium-accuracy OIUS-501 FOGs. The random component of the zero bias of FOGs of this type is 0.3°/h. It is significantly higher than the requirements in the specification for the stabilization accuracy of most satellites, and remote sensing satellites, in particular.

The challenge is to create a high-precision strapdown inertial system, the accuracy of which will be almost several times higher than that of the available sensors, which is only possible due to the application of ground calibrations, a special mathematical analysis of measurements, and additional in-flight orbital calibration aboard the satellite.

---

[1] PhD, CEO.
[2] Chief of Department.
[3] PhD, Chief of Test and Certification Center.
[4] PhD, Associate Professor, Chief of Sector.
[5] Lead Engineer and Mathematician.
[6] Doctor Sciences (Engineering), Professor.
[7] Lecturer.

Objective

Application of FOGs as ARS's posed a number of new challenges for designers: to study the effects of temperature, magnetic field and radiation on FOG measurement errors, to develop methods for improving the FOG technology and test methodology for determining their technical characteristics, and to develop mathematical models.

The aim of the research discussed in this paper is, firstly, to develop a methodology of ground and orbital calibration work for the determination of fiber-optic gyroscopes measurement error and inertial measurement unit error altogether for their algorithmic board compensation in special computer. Secondly, the methodology testing on a real device, and evaluation of the results of its application in the form of the achieved accuracy characteristics of the developed inertial measurement block.

To achieve this aim, the following objectives were posed and solved in the work:

- to study the magnetic sensitivity of FOG;
- to study temperature sensitivity of FOG and, if necessary, create a mathematical model of the temperature drift (thermal calibration);
- to carry out the calibration in order to determine FOG zero bias which does not depend on the temperature factor, scale factor and errors in manufacturing sensitive elements and IMU;
- to develop a methodology of orbital calibration;
- to estimate the effectiveness of the methods developed to achieve the accuracy characteristics.

Step-by-step solution of these problems is the basis for implementing the technology for creation of a high-precision strapdown FOG-based IMU for an integrated control system.

The initial steps are carried out during ground-based operations, whereas the final steps, aimed at providing additional increase in accuracy, are performed during in-flight operation of the SINS as a part of a satellite control system.

The IMU for space applications consists of four FOGs, the unit for rocket applications, of three FOGs and three pendulum accelerometers. The FOGs and accelerometers are mounted on a base platform according to the orthogonal scheme. The fourth FOG of the IMU for space applications is mounted so that its axis of sensitivity makes equal angles with the axes of sensitivity of the first three FOGs.

The exterior view of the strapdown inertial system for space applications with the cover removed is shown in Fig. 1.

Fig. 1. Exterior view of the strapdown inertial system

Studying the FOG magnetic sensitivity

Preliminary estimations of the biases of the sensors, which differ both in magnitudes and signs, were made in the RPE Hartron-Arkos as a result of the input control of OIUS-501-type FOG. Since a testbed implements sufficient accuracy for a given direction of the axes of the sensors, it was suggested that the main reason for the substantial differences in the results obtained is the FOG measurement sensitivity to the external magnetic field, namely, to the Earth's magnetic field, and to the field generated by the surrounding equipment [4, 5]. A method of experimental investigation of the effect produced by the external magnetic field on the measurement error was developed to confirm this hypothesis and to obtain quantitative characteristics.

The method consists in determining the magnetic sensitivity of FOG by approximating the measurement errors of projections of the angular velocity of the Earth on the sensitive axes (SA) of FOGX and FOGY of the IMU for different fixed values of the azimuth angle ψ_i ($i = 1, 2, ..., 25$) given by the IMU rotation on a swivel rotary table in the plane of the local horizon with increments of 15°. The angle ψ is measured from north direction till the sensitive axis of FOGX. FOG measurements (channels X and Y) were carried out in 25 fixed positions of the IMU when the angle ψ_i was changed from 0° to 360° [5, 6].
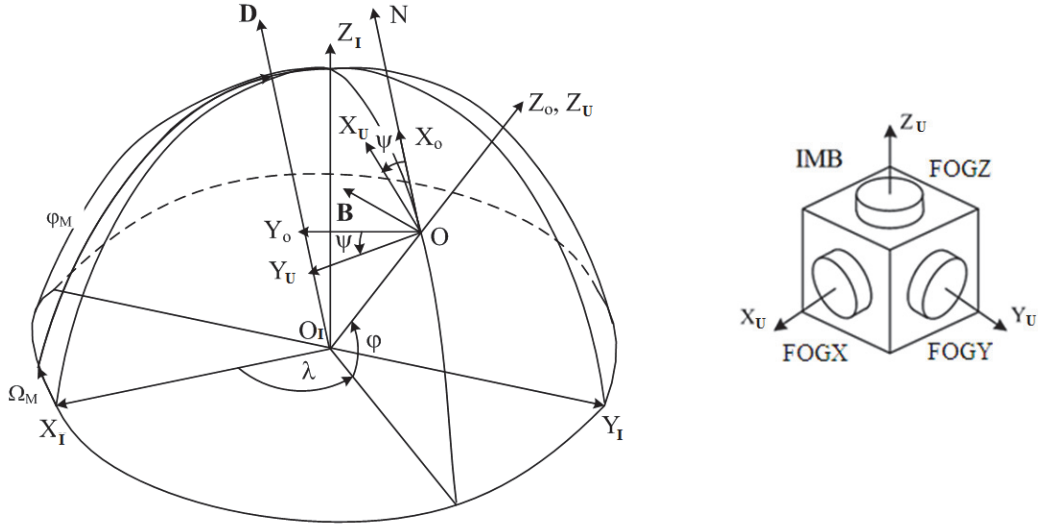
The scheme of magnetic tests of the IMU is shown in Fig. 2.

Fig. 2. The scheme of magnetic tests of the IMU

Fig. 2 shows:
$O_IX_IY_IZ_I$ – second equatorial (inertial) coordinate system (2ECS);
$OX_OY_OZ_O$ – local orbital coordinate system (OCS);
$OX_PY_PZ_P$ – instrumental coordinate system (ICS), fixed to the IMU;
λ, φ – local longitude and latitude;
ψ – azimuthal angle of the IMU;
N – the direction of north pole of the Earth;
Ω_M, φ_M – the angles determining the position of vector of the Earth's magnetic dipole moment **D** in the 2ECS;
B – the induction vector of the Earth's magnetic field (EMF).

According to the results of magnetic tests of OIUS-501-type FOG, the value of the measurement error caused by the effect of the external magnetic field is significant and it may be from ±0.05 to $0.15°/h$ [2]. However, the question of how the FOG orientation in the external magnetic field, particularly, in the EMF, affects FOG measurement errors has not been adequately studied.

Consider the variation of FOG magnetic sensitivity depending on the relative orientation of the Earth's magnetic field induction **B** and the FOG sensitivity axis.

In accordance with the results of the magnetic tests, the measurement errors of FOGX and FOGY of the IMU can be approximated by periodic functions $f_j(\psi)$, $(j=x,y)$ of the form [2]:

$$f_x(\psi) = \delta\Omega_x + S_x\sin(\psi+\Delta\varphi_x); \quad f_y(\psi) = \delta\Omega_y + S_y\cos(\psi+\Delta\varphi_y), \tag{1}$$

where $\delta\Omega_j$, S_j, $\Delta\varphi_j$ $(j=x,y)$ are the estimate of constant systematic zero bias, amplitude and phase shift of periodic component of the measurement error of FOGJ (J = X, Y); ψ – an azimuthal angle of FOGX.

The parameter values of functions $f_x(\psi)$ and $f_y(\psi)$ were obtained from the FOG tests without a screen and with a screen. Then the approximating functions describing the magnetic component for FOGX and FOGY were obtained as:

$$\Delta f_x(\psi) = \Delta\Omega_x + \Delta S_x\sin(\psi + \Delta\varphi_x); \quad \Delta f_y(\psi) = \Delta\Omega_y + \Delta S_y\cos(\psi + \Delta\varphi_y), \tag{2}$$

where $\Delta f_j(\psi)$, $\Delta\Omega_j$, ΔS_j $(j=x,y)$ – the differences between the functions and the corresponding components obtained in the FOG tests without a screen and with a screen.

Now let us determine at which mutual orientation of the FOGX and FOGY SAs in relation to the Earth's magnetic field induction vector **B** functions (2) have maximum and minimum.

The projection of $\mathbf{B}_0 = \{B_{0j}\}$ $(j=x,y,z)$ at the test point on the axis of the local OCS is calculated by the formulas of the mathematical model of the EMF simulated as a "dipole tilt" [7]:

332

$$B_{0X} = B_0 \sin \xi_{_M} \sin(u - \eta_{_M});$$
$$B_{0Y} = B_0 \cos \xi_{_M};$$
$$B_{0Z} = -2B_0 \sin \xi_{_M} \cos(u - \eta_{_M}),$$

where $\sin \xi_{_M} = \sqrt{1 - (\sin \varphi_{_M} \cos i + \cos \varphi_{_M} \sin i \sin \Omega_{_\Sigma})^2}$; $\eta_{_M} = \mathrm{arctg} \dfrac{\sin \varphi_{_M} \sin i - \cos \varphi_{_M} \cos i \sin \Omega_{_\Sigma}}{\cos \varphi_{_M} \cos \Omega_{_M}}$.

There B_0 – the value of modulus of vector $\boldsymbol{B_0}$ at the magnetic equator; u – the argument of latitude; i – an inclination; $\varphi_{_M}$, $\Omega_{_M}$ – the angles determining the position of vector of the magnetic dipole moment of the Earth in 2ECS; $\Omega_{_\Sigma} = \Omega_{_M} + \Omega - (\omega_E + \dfrac{d\Omega}{dt})t$; Ω – the longitude of orbit ascending node; ω_E – the angular velocity of the Earth's rotation; $\dfrac{d\Omega}{dt}$ – the angular velocity of precession of the orbit; $\xi_{_M}$ – an orbital inclination to the magnetic equator; $\eta_{_M}$ – an angle between the ascending node in the planes of the geographic and magnetic equators.

It is known that the south pole of EMF has the offset 11.5° in relation to the geographic north Pole of the Earth, and it has the following coordinates: lat. 78.5° N and long. 69.1°W. The latitude φ and the longitude λ of location where the tests occurred in Kharkov are respectively 50°03′ and 36°17′. The inclination i is 90° in this case.

Given that EMF rotates with the Earth, we calculate the projection of $\boldsymbol{B_0}$ at time 00 h 00 min 00 s. Then $\Omega_{_\Sigma} = \Omega_{_M} + \Omega$ or $\Omega_{_\Sigma} = \Omega_{_M} + \lambda$, where $\lambda = \Omega$ is the local longitude.

For the following numerical values of the initial data: $B_0 = 31 \cdot 10^3$ nT; $\varphi_{_M} = 78.5°$; $\Omega_{_M} = 69.1°$; $\lambda = 36°17′$; $u = \varphi = 50°03′$; $i = 90°$ we obtain $B_{0X} = 21846.0$ nT; $B_{0Y} = 5967.0$ nT; $B_{0Z} = -42340.0$ nT.

The projections of vector $\boldsymbol{B_0}$ in IMU ICS are as follows:

$$\mathbf{B_\Pi} = \begin{bmatrix} B_{\Pi X} \\ B_{\Pi Y} \\ B_{\Pi Z} \end{bmatrix} = \begin{bmatrix} \cos \psi & \sin \psi & 0 \\ -\sin \psi & \cos \psi & 0 \\ 0 & 0 & 1 \end{bmatrix} \cdot \begin{bmatrix} B_{0X} \\ B_{0Y} \\ B_{0Z} \end{bmatrix} = \begin{bmatrix} B_{0X} \cos \psi + B_{0Y} \sin \psi \\ -B_{0X} \sin \psi + B_{0Y} \cos \psi \\ B_{0Z} \end{bmatrix}.$$

The relative angular position of FOGJ, namely the sensitivity axis OVJ (J = X, Y), in relation to the vector $\boldsymbol{B_\Pi} = \{B_{\Pi j}\}$ ($j = x, y, z$) we estimate by the formula

$$\cos \alpha_j = (\mathbf{B_\Pi}, \mathbf{OVJ}) = \sum_j B_{\Pi j} OVJ_j \quad (j = x, y). \tag{3}$$

Given the FOGJ position in IMU ICS, at which $\mathbf{OVX} = (1, 0, 0)^T$, $\mathbf{OVY} = (0, 1, 0)^T$, we get

$$\cos \alpha_j = \frac{B_{\Pi j}}{|\mathbf{B_\Pi}|}, \quad B_0 = |\mathbf{B_0}| = \sqrt{\sum_{j=x,y,z} B_{0j}^2} \cdot \qquad (j = x, y)$$

The conditions of extremum for functions (2) are the follows:

$$\frac{\partial[\Delta f_x(\psi)]}{\partial \psi} = \Delta S_x \cos(\psi + \Delta \varphi_x) = 0, \qquad \frac{\partial[\Delta f_y(\psi)]}{\partial \psi} = -\Delta S_y \sin(\psi + \Delta \varphi_y) = 0 \cdot$$

From these conditions we get that $\max|\Delta f_x(\psi)|$ takes place in the vicinity of angles $\psi = \pi/2 - \Delta \varphi_x$, $3\pi/2 - \Delta \varphi_x$, and $\max|\Delta f_y(\psi)|$ – at $\psi = 0 - \Delta \varphi_y$, $\pi - \Delta \varphi_y$, $2\pi - \Delta \varphi_y$.

According to the tests it is determined that the phase angle $\Delta \varphi_j$ ($j = x, y$) is about -15°. Then from (3) we obtain that the maximum sensitivity of FOGX and FOGY are revealed in the vicinity of angles $\alpha_{x,y} = 90 \pm 3°$.

Solving the inverse problem of finding the phase shift of the azimuthal angle of the magnetic component in the FOG measurement errors, when $\alpha_j = 90°$ ($j = x, y$) at the points of maximum sensitivity of FOG, we obtain

$$\Delta \varphi_{x,y} = -arctg \frac{B_{0Y}}{B_{0X}} \cdot$$

And the values of projections B_{0X}, B_{0Y} on the test location place give that the phase angle $\Delta\varphi_j$ is -15.3°. This result with sufficient accuracy coincides with the value of the angle obtained from the experimental data.

Therefore, we can conclude that the maximum sensitivity of FOG takes place under the action of induction vector of external magnetic field orthogonal to FOG sensitivity axis, i.e. in the plane of fiber loop. At the same time, we note that the sign of magnetic component of FOG error depends on direction of action of external magnetic field induction vector. So, for example, for FOGX at a value $\psi=\pi/2-\Delta\varphi_x$ the magnetic error is maximum and positive, while at a value $\psi=3\pi/2-\Delta\varphi_x$ the magnetic error is negative.

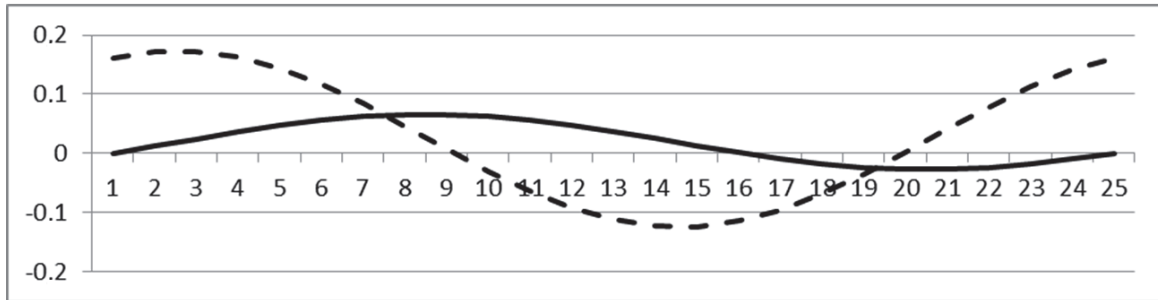The graphs of functions $\Delta f_j(\psi)$ and angles $\alpha_j(\psi)$ ($j=x, y$) are shown in Fig. 3 and Fig. 4.

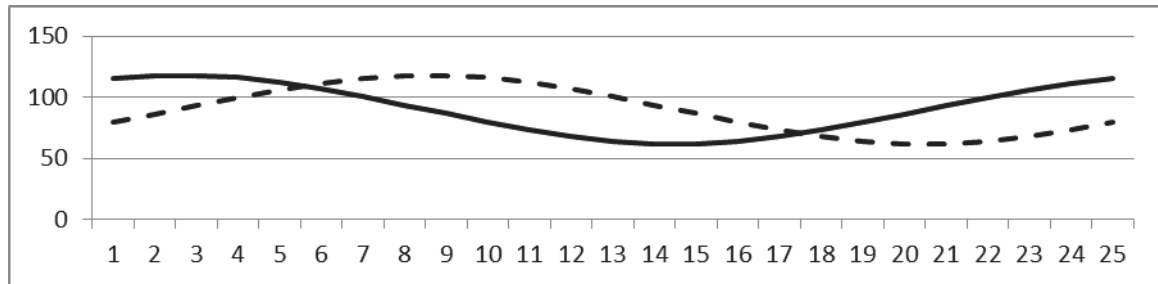Fig. 3. Function $\Delta f_j(\psi)$: solid – $\Delta f_x(\psi)$, deg/h; dotted – $\Delta f_y(\psi)$, deg/h

Fig. 4. Angles $\alpha_j(\psi)$: solid – $\alpha_x(\psi)$, deg; dotted – $\alpha_y(\psi)$, deg

On the x-axis the azimuth angle ψ postponed by numbers of points at which the measurements of FOG in the magnetic tests were carried out: ψ= -141.5°at point 1, ψ = -156.5° at point 2, etc. till IMU completes turn at 360°.

Consider the explanation for dependence of FOG magnetic sensitivity on its orientation.

Magnetic sensitivity of FOG is a consequence of the Faraday effect – an interaction between light and a magnetic field in a medium. The Faraday effect causes a rotation of the plane of polarization of light traveling in the fiber loop of FOG, under the action of an external magnetic field on device [8]. Under the action of external magnetic field induction vector along FOG SA the changes of the polarization plane of light rays forward and reverse occurs equally. Under the action of external magnetic field induction vector in the plane of fiber loop the changes of the polarization plane of light rays in distant orbits of fibers occurs weaker than in nearby orbits, which causes additional phase shift when adding light in photodetector and thus generates an additional shift of the zero signal of FOG.

Thus, the maximum effect of the action takes place when induction vector of external magnetic field is orthogonal to FOG SA, i.e. in the plane of fiber loop. The sign of magnetic component of FOG error depends on the direction of action of external magnetic field vector.

We should consider the impact of inventories during ground tests of FOG. This is accomplished by selecting the appropriate orientation of the device. If this is difficult to do during FOG tests comprising IMU, for example, during ground calibration, the devices must be securely shielded or placed into the apparatus, which compensate the effect of the EMF.

The main result of studying the magnetic sensitivity of OIUS-501-type FOG is the fact that FOGs from new batch, received by RPE Hartron-Arkos, were performed in a shell with good magnetic protection. This was confirmed by repeated magnetic tests of new devices [6].

Studying FOG temperature sensitivity

Temperature is one of the major factors affecting the accuracy of FOG [2, 8]. Therefore, the main task in the problem of improving the accuracy of IMU, generated on the base of FOG, is the task of constructing a mathematical model of FOG temperature drift. In accordance with the methodology developed by the company for devices (from the first batch) of medium accuracy class of OIUS-501-type the thermal tests were conducted. A third-order polynomial with constant coefficients mathematical model was developed. The model explains the dependence of the displacement of the FOG zero signal on temperature and its gradient. The application of this model for algorithmic compensation of FOG temperature drift allows reducing the systematic component of zero offset, depending on temperature factor [2, 9].

For the second batch of FOG the dependence of measurement error on temperature and its gradient was not as obvious as for the first batch (see graphs in Fig. 5). Abscissa of the graphs is time in minutes.

a)
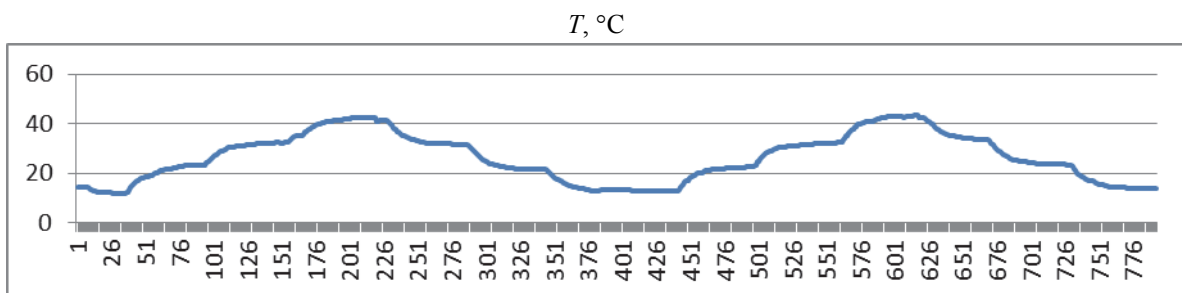
b)
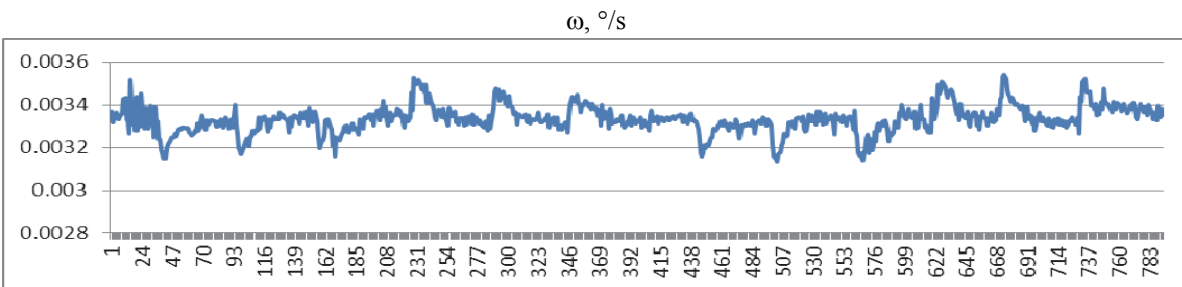
c)
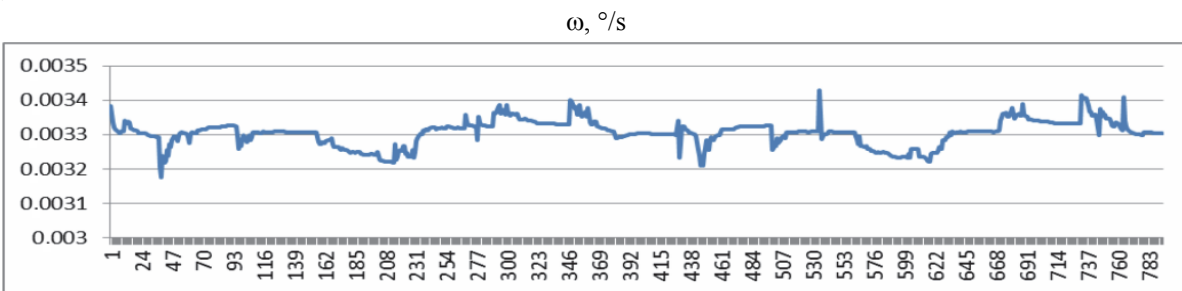
c)

Fig. 5. The cyclogram of temperature variation (a), and output signals of FOG for the first (b) and second (c) batches

The item on the preliminary analysis of data for thermal tests of FOG was included to the methodology of constructing the compensation models of FOG thermal error. The goal of this item is to provide a rigorous answer to the question whether there is dependence of FOG measurement errors on temperature or this dependence is negligible.

Studying the first batch of FOG leads to the following conclusion: the method of two-factor analysis of variance should be applied. As a first factor the temperature should be taken, and as a second factor – the rate of change, i.e. temperature gradient.

In accordance with the plan of the experiment and usage of two-factor analysis of variance the resulting thermal test data can be represented in Table 1 [10].

T a b l e 1

The representation of the results of thermal tests

The numbers and values of the factor levels			G, °C/min							
			1		2				3	
			-0.25		0				0.25	
			1	2	1	2	3	4	1	2
T, °C	1	10	-		$\omega_{121}^{(1)}$ ... $\omega_{12i}^{(1)}$ ... $\omega_{12N}^{(1)}$	$\omega_{121}^{(2)}$ ... $\omega_{12i}^{(2)}$ ... $\omega_{12N}^{(2)}$	$\omega_{121}^{(3)}$ ... $\omega_{12i}^{(3)}$ ... $\omega_{12N}^{(3)}$	$\omega_{121}^{(4)}$ ... $\omega_{12i}^{(4)}$ ... $\omega_{12N}^{(4)}$	$\omega_{131}^{(1)}$ ... $\omega_{13i}^{(1)}$ ... $\omega_{13N}^{(1)}$	$\omega_{131}^{(2)}$ ... $\omega_{13i}^{(2)}$ ... $\omega_{13N}^{(2)}$
	2	20	$\omega_{211}^{(1)}$ ... $\omega_{21i}^{(1)}$ ... $\omega_{21N}^{(1)}$	$\omega_{211}^{(2)}$ ... $\omega_{21i}^{(2)}$ ... $\omega_{21N}^{(2)}$	$\omega_{221}^{(1)}$ ... $\omega_{22i}^{(1)}$ ... $\omega_{22N}^{(1)}$	$\omega_{221}^{(2)}$ ... $\omega_{22i}^{(2)}$ ... $\omega_{22N}^{(2)}$	$\omega_{221}^{(3)}$ ... $\omega_{22i}^{(3)}$ ... $\omega_{22N}^{(3)}$	$\omega_{221}^{(4)}$ ... $\omega_{22i}^{(4)}$ ... $\omega_{22N}^{(4)}$	$\omega_{231}^{(1)}$ ... $\omega_{23i}^{(1)}$ ... $\omega_{23N}^{(1)}$	$\omega_{231}^{(2)}$ ... $\omega_{23i}^{(2)}$ ... $\omega_{23N}^{(2)}$
	3	30	...	...	...	...	...	...	...	...
	4	40	$\omega_{411}^{(1)}$ ... $\omega_{41i}^{(1)}$ ... $\omega_{41N}^{(1)}$	$\omega_{411}^{(2)}$ ... $\omega_{41i}^{(2)}$ ... $\omega_{41N}^{(2)}$	$\omega_{421}^{(1)}$ ... $\omega_{42i}^{(1)}$ ... $\omega_{42N}^{(1)}$	$\omega_{421}^{(2)}$ ... $\omega_{42i}^{(2)}$ ... $\omega_{42N}^{(2)}$	-		-	

Table 1 shows:

T – temperature, °C; G – temperature gradient, °C/min; $\omega_{jgi}^{(k)}$ – i-th measuring of FOG on the k-th plot (i=1, 2,..., N; k=1, 2, …, m_v, m_v=2 or m_v=4); N – number of measuring of FOG during a 20-minute interval; j – number of levels of the first factor (j = 1, 2, 3, 4); g – number of levels of the second factor (g = 1, 2, 3).

If the duration of tact T_0 of apparatus survey of FOG is 5 ms, then the number N of measurements on the 20-minute interval will be 240000.

The FOG measurement error is calculated by the formula:

$$Y_{jgi}^{(k)} = \omega_{jgi}^{(k)} - \omega^*,$$

where $\omega^* = \omega_E \sin\varphi = 11.530190°$/h – the reference value of angular velocity measured by FOG;

$\omega_E = 15.041068°$/h – the angular velocity of Earth's rotation;

$\varphi = 50°2'52.64'' = 50.0480°$ – the local latitude.

Using data from Table 1 we determine the average values of the FOG measurements errors on m_v plots for each of ten experiments:

$$Y_{jgi} = \frac{1}{m_v}\sum_{k=1}^{m_v} Y_{jgi}^{(k)}.$$

Table 1 can be written in the form of representation adopted for two-factor analysis of variance for mean values in the plots of FOG measurement errors [10]; the mean by rows, columns, and the total average of all observations can be calculated for all combinations of levels by the formulas:

$$\overline{Y}_j = \frac{1}{n_g N}\sum_g\sum_i Y_{jgi}, \quad \overline{Y}'_g = \frac{1}{n_j N}\sum_j\sum_i Y_{jgi}, \quad \overline{\overline{Y}} = \frac{1}{M}\sum_j\sum_g\sum_i Y_{jgi},$$

where $M = nN$ – the number of observations for all n combinations of levels.

The designation are as follows:

- for $\overline{Y}_j$ $j=1, 2, 3, 4$;

$$g = \begin{cases} 2, 3, & \text{for } j = 1, \\ 1, 2, 3, & \text{for } j = 2 \vee 3, \\ 1, 2, & \text{for } j = 4; \end{cases} \quad n_g = \begin{cases} 2, & \text{for } j = 1 \vee 4, \\ 3, & \text{for } j = 2 \vee 3; \end{cases}$$

- for $\overline{Y}'_g$ $g=1, 2, 3$;

$$j = \begin{cases} 2, 3, 4, & \text{for } g = 1, \\ 1, 2, 3, 4, & \text{for } g = 2, \\ 1, 2, 3, & \text{for } g = 3; \end{cases} \quad n_j = \begin{cases} 3, & \text{for } g = 1 \vee 3, \\ 4, & \text{for } g = 2. \end{cases}$$

The evaluations of the variances are calculated with the appropriate degrees of freedom [10]:

$$s_0^2\{Y\} = \frac{1}{M-1}\sum_j\sum_g\sum_i (Y_{jgi} - \overline{\overline{Y}})^2, \quad \nu_0 = M - 1,$$

$$s_\varepsilon^2\{Y\} = \frac{1}{n}\sum_j\sum_g \frac{1}{N-1}\sum_i (Y_{jgi} - \overline{Y}_{jg})^2, \quad \text{where } \overline{Y}_{jg} = \frac{1}{N}\sum_{i=1}^{N} Y_{jgi}, \quad \nu_\varepsilon = n(N-1),$$

$$s_T^2\{Y\} = \frac{u_2 N}{u_1 - 1}\sum_{j=1}^{u_1} (\overline{Y}_j - \overline{\overline{Y}})^2, \quad \nu_T = u_1 - 1, \quad \text{where } u_1, u_2 - \text{the number of levels of factors,}$$

$$s_G^2\{Y\} = \frac{u_1 N}{u_2 - 1}\sum_{g=1}^{u_2} (\overline{Y}'_g - \overline{\overline{Y}})^2, \quad \nu_G = u_2 - 1,$$

$$s_{TG}^2\{Y\} = \frac{N}{\nu_{TG}}\sum_j\sum_g (\overline{Y}_{jg} - \overline{Y}_j - \overline{Y}'_g + \overline{\overline{Y}})^2, \quad \nu_{TG} = \nu_0 - \nu_\varepsilon - \nu_T - \nu_G.$$

The evaluation of significance of influence of factors and their interaction is carried out by comparing the ratio of variances with their critical values. The null hypothesis of the effect of T and G factors and their interactions on the FOG measurement error is checked by confirming the following inequalities:

$$F_T = \frac{s_T^2\{Y\}}{s_{TG}^2\{Y\}} > F_q(\nu_T; \nu_{TG}), \quad F_G = \frac{s_G^2\{Y\}}{s_{TG}^2\{Y\}} > F_q(\nu_G; \nu_{TG}), \quad F_{TG} = \frac{s_{TG}^2\{Y\}}{s_\varepsilon^2\{Y\}} > F_q(\nu_{TG}; \nu_\varepsilon).$$

The numerical results of statistical treatment of the FOG measurement errors for the first (I) and second (II) batches that were obtained from data of thermal tests are shown in Table 2.

T a b l e 2

The ratio of variances and the critical values

Notation	Ratio of variances		Critical values	
	I	II	q=5%	q=1%
F_T	8.17	6.03	6.59	16.69
F_G	20.42	19.51	6.94	18.00
F_{TG}	26.02	21.69	2.32	3.32

As follows from the results, the effect of temperature factor is significant for FOGs from the first batch and is absent for FOGs from the second batch (at q=5%). A strong influence of the temperature gradient was observed for FOGs from the both batches. Also observed was a significant joint effect of two factors: temperature and its gradient.

For the FOG from the first batch the construction of temperature drift models is effective. For the FOG from the second batch, this process is inefficient.

The studies lead to the following conclusions.

Firstly, it is not the temperature but its variation, i.e., gradient, that produces the most significant effect.

Secondly, at the initial stage of processing the data from the thermal experiments aimed at constructing a mathematical model of FOG temperature drift, one should previously examine the data in accordance with the method of two-factor analysis of variance. If the effect of thermal factors on the FOG measurement errors is confirmed, the FOG temperature drift model is worth constructing, otherwise, there is no sense in constructing it.

Ground calibration of the FOG SA position

The purpose of this phase of ground calibration is to refine the actual orientation of the FOG SAs after the FOGs are placed inside the IMU. A specific feature of the problem is the presence of the fourth FOG, for which, due to its spatial location, it is difficult to implement a calibrating rotation with the axis close to its own SA. Therefore it was necessary to develop a methodology for performing the calibration experiments and processing information taking into consideration the available stand equipment.

Two methods have been developed. The first method was based on direct measurements of FOG and on comparing the values of the angle turn in uniaxial rotation with a reference one. The first method allows a refinement of misalignment of angles up to 30″. The maximum contribution to the error don't make a full account of systematic drift of FOG. The second method is developed using the algorithm of SINS after recompense of "rough" errors established by the first method. The residual error after application of the second method is approximately 5″. The second method has been implemented only to refine the parameters of misalignment of orthogonal triple of FOG.

The first method. Let $X_\Pi Y_\Pi Z_\Pi$ be an instrument coordinate system of IMU; $X_i Y_i Z_i, i = \overline{1,4}$ – a coordinate system associated with FOG, axis Z_i is directed along the SA of i-th FOG.

We define the orientation of the FOG1 SA relative to the ICS as a result of two consecutive turns (Fig. 6a):

1. The rotation of the axis X_Π counterclockwise by an angle $\delta13$ about the axis Z_Π;

2. The counterclockwise rotation of the transformed axis X'_Π by an angle $\delta12$ around the axis Y'_Π.

Define FOG4 axis orientation, oppositely directed to SA as a result of two consecutive turns (Fig. 6b):

1. The rotation of the axis X_Π counterclockwise by an angle $\alpha = \pi/4 + \delta43$ about the axis Z_Π;

2. The clockwise rotation of the transformed axis X'_Π by an angle $\beta = (\gamma - \pi/2) - \delta42$ around the axis Y'_Π where $\gamma = 2.186276$ rad (125°15′52″).
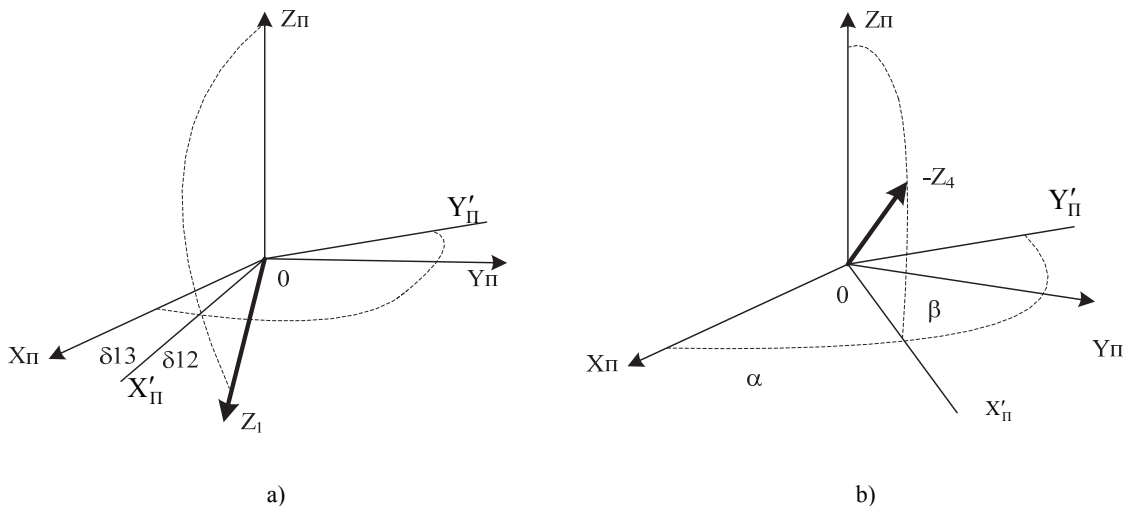
Fig. 6. Orientation of FOG1 SA (a) and FOG4 SA (b) relative to the ICS

The misalignment parameters for FOG2 and FOG3 are entered by the same way as for FOG1. In this case the problem of calibration is to determine eight parameters $\delta12, \delta13, \delta21, \delta23, \delta31, \delta32, \delta42, \delta43$, describing the deviation of SA from their nominal position.

Three turning at some fixing angle, that will be completed consequentially, are the basis for solving the problem by direct measurements. Bringing the corresponding axis of ICS in a vertical position precedes reversal.

The system of equations is formed by the results of measurements:

$$\Theta_{Y\Pi}^{(k)} \cdot \delta13 - \Theta_{Z\Pi}^{(k)} \cdot \delta12 = \Theta_1^{(k)} - \delta\omega_1^* \cdot T^{(k)} - \Theta_{X\Pi}^{(k)},$$

$$-\Theta_{X\Pi}^{(k)} \cdot \delta23 + \Theta_{Z\Pi}^{(k)} \cdot \delta21 = \Theta_2^{(k)} - \delta\omega_2^* \cdot T^{(k)} - \Theta_{Y\Pi}^{(k)},$$

$$\Theta_{X\Pi}^{(k)} \cdot \delta32 - \Theta_{Y\Pi}^{(k)} \cdot \delta31 = \Theta_3^{(k)} - \delta\omega_3^* \cdot T^{(k)} - \Theta_{Z\Pi}^{(k)},$$

$$(c_\gamma \cdot \Theta_{Z\Pi}^{(k)} - s_{\gamma2} \cdot (\Theta_{X\Pi}^{(k)} + \Theta_{Y\Pi}^{(k)})) \cdot \delta42 + c_{\gamma2} \cdot (\Theta_{X\Pi}^{(k)} - \Theta_{Y\Pi}^{(k)}) \cdot \delta43 =$$
$$= \Theta_4^{(k)} - \delta\omega_4^* \cdot T^{(k)} + c_{\gamma2} \cdot \Theta_{X\Pi}^{(k)} + c_{\gamma2} \cdot \Theta_{Y\Pi}^{(k)} + s_\gamma \cdot \Theta_{Z\Pi}^{(k)}$$

in which $k = \overline{1,3}$ – a number of calibration turn; $\Theta_1^{(k)}$, $\Theta_2^{(k)}$, $\Theta_3^{(k)}$, $\Theta_4^{(k)}$ – the angles of rotation in the *k*-th turn, calculated as the sum of the measurements of angular velocity of FOG, multiplied by the tact of data refresh. The summation is carried out over time $T^{(k)}$ – the duration of calibration circle; $\delta\omega_1^*$, $\delta\omega_2^*$, $\delta\omega_3^*$, $\delta\omega_4^*$ – the evaluation of systematic drift of FOG obtained in the steady state in the start position in the certified IMU; $c_\gamma = 0.816497$, $s_\gamma = 0.577350$, $c_{\gamma2} = 0.577351$, $s_{\gamma2} = 0.408248$ – the constants; $\Theta_{X\Pi}^{(k)}$, $\Theta_{Y\Pi}^{(k)}$, $\Theta_{Z\Pi}^{(k)}$ – the reference values of the angles of rotation around the axis of the ICS calculated at the initial value of the azimuth ψ_0: for *k*=1 by the formulas $\Theta_{X\Pi}^{(1)} = \frac{\Omega_N}{\omega^*} \cdot (\sin(\psi_0) - \sin(\psi_0 - \Theta_T^*))$, $\Theta_{Y\Pi}^{(1)} = \frac{\Omega_N}{\omega^*} \cdot (\cos(\psi_0 - \Theta_T^*) - \cos(\psi_0))$, $\Theta_{Z\Pi}^{(1)} = \Omega_H \cdot T + \Theta_T^*$, in which Θ_T^* – the measuring angle of rotation, its sign coincides with the sign of the reference angular velocity ω^*; $T = \Theta_T^* / \omega^*$ – the duration of a turn; for *k*=2 according to the formulas $\Theta_{X\Pi}^{(2)} = \Omega_H \cdot T + \Theta_T^*$, $\Theta_{Y\Pi}^{(2)} = \frac{\Omega_N}{\omega^*} \cdot (\sin(\psi_0) - \sin(\psi_0 - \Theta_T^*))$, $\Theta_{Z\Pi}^{(2)} = \frac{\Omega_N}{\omega^*} \cdot (\cos(\psi_0 - \Theta_T^*) - \cos(\psi_0))$; for *k*=3 by the formulas $\Theta_{X\Pi}^{(3)} = \frac{\Omega_N}{\omega^*} \cdot (\cos(\psi_0 - \Theta_T^*) - \cos(\psi_0))$, $\Theta_{Y\Pi}^{(3)} = \Omega_H \cdot T + \Theta_T^*$, $\Theta_{Z\Pi}^{(3)} = \frac{\Omega_N}{\omega^*} \cdot (\sin(\psi_0) - \sin(\psi_0 - \Theta_T^*))$; $\Omega_N, \Omega_H, \Omega_E$ – the north, vertical, and east velocity components of Earth's rotation.

Solving the reduced system by the least square method, we obtain the desired angles $\delta12$, $\delta13$, $\delta21$, $\delta23$, $\delta31$, $\delta32$, $\delta42$, $\delta43$.

This methodology works for any platform stand's turning angle and rotational velocity. It also takes into account the effect of Earth's angular velocity and systematic drifts.

Implementing this methodology requires the following:
- Gyroscopic measurements;
- Estimates of systematic drifts at launch;
- Initial azimuth at each calibration turn;
- Reference value of the angular velocity of platform rotations for each calibration turn;
- Reference value of the turn angle for each calibration turn;
- Locational latitude.

Requirements for experimental conditions are as follows:
- Proper leveling of IMU ICS;
- Absence of the precession of the rotation axis;
- Highly accurate initial alignment of ICS axes;
- Accurate time measures of realized rotation angle.

The second method. The second method of calibration – using the SINS algorithm – is described here in general terms only. To accurately detect the misalignment using the SINS algorithm requires the following:
- The non-orthogonality should not too large (up to 1′) due to the fact that the error measuring models are based on linearized equations; thus, the method applies when seeking the parameters by direct gyroscopic measurements;
- The flat-turn IMU, offered in this methodology, should not be too long to reduce the impact on the accuracy of non-orthogonality parameters, of the FOG's uncompensated systematic drift;
- It is possible to refine two non-orthogonality parameters of horizontal axes of IMU in one single installation; to determine all six parameters of FOG1, FOG2 and FOG3 axes requires three installations of IMU

(1st installation with Z ICS axis up; 2nd installation with X ICS axis up, and third – Y ICS axis up) and three measurement cycles respectively.

This method is based on the fact that the non-orthogonality of FOG SA may lead to "rapid" changes in computation errors of SINS orientation angles when SA is rotated. Breaking the task into subtasks leads to the choice of rotational types – flat turn, vertical axis or a turn angle (180°). This decision on rotational types is also influenced by the fact that turning 180° substantially impacts the errors. This last point follows from the analytical basis of this methodology.

Advantages of using the SINS algorithm on direct measurements follow from the fact that the result does not depend on the

- Rotational instability and the rotation precession swing of the platform axis;
- Earth's rotation, during the measurement cycle, is accurately computed;
- Low required accuracy of implementation of the angle of rotation.

The metrological support of this methodology includes:

- Deflection angles of ICS's horizontal axes from the horizontal plane, both in the initial platform position and its reverse position, after a 180° rotation over the vertical axis. Note that the non-orthogonality parameters' measurement error equals the error of setting those angles;

- Starting position of the platform must be such that one of the horizontal axes of the ICS is directed northwards.

To validate the parameters obtained through the use of this methodology, one should assess the repeatability of parameters of non-orthogonality on multiple runs of IMU. It is possible also to use the application determination algorithm to calculate the final orientation of IMU and to compare it with the reference measurements, with and without the inclusion of non-orthogonal parameters. Obtaining a lower orientation error in the second case evidences the reliability of results.

Combining both methods for ground calibration of the positions of FOG sensitivity axes allows achieving sufficient accuracy required for the instrument as a whole to be used for orbit calibration.

The methodology of orbital calibration

Statement of the problem. Questions like these were considered in [11-14]. Consider the calibration of IMU during flight of the satellite in orbit. The challenge is determining the scaling factors and FOG zero bias, the deterministic error misalignment of FOG sensitivity axes and star tracker used for stellar correction of IMU.

The measurement models of FOG and star tracker are presented by the formulas:

$$\boldsymbol{\omega}^*(t) = \boldsymbol{\omega}(t) + \boldsymbol{\delta\omega}^*(t), \tag{4}$$

$$\boldsymbol{\Lambda}^*(t) = \boldsymbol{\Lambda}(t) \circ \boldsymbol{\delta\Lambda}^*. \tag{5}$$

Here the vectors of FOG measurement errors $\boldsymbol{\delta\omega}^*(t)$ and star tracker measurement errors $\boldsymbol{\delta\Lambda}^*$ are presented in the form:

$$\boldsymbol{\delta\omega}^*(t) = \boldsymbol{\Delta\omega} + (-\boldsymbol{\delta K_\omega} + \boldsymbol{\delta\Psi_\omega}) \cdot \boldsymbol{\omega}(t) + \boldsymbol{\xi_\omega}(t),$$

$$\boldsymbol{\delta\Lambda}^* = \boldsymbol{\delta\Psi_\Lambda} \circ \boldsymbol{\delta\Xi},$$

where $\boldsymbol{\Delta\omega} = (\Delta\omega_x; \Delta\omega_y; \Delta\omega_z)^T$ – the vector of zero bias; $\boldsymbol{\delta K_\omega} = \begin{pmatrix} \delta K_{\omega x} & 0 & 0 \\ 0 & \delta K_{\omega y} & 0 \\ 0 & 0 & \delta K_{\omega z} \end{pmatrix}$ – the matrix of the error of

scale factors; $\boldsymbol{\delta\Psi_\omega} = \begin{pmatrix} 0 & \delta\Psi_{\omega xy} & -\delta\Psi_{\omega xz} \\ -\delta\Psi_{\omega yx} & 0 & \delta\Psi_{\omega yz} \\ \delta\Psi_{\omega zx} & -\delta\Psi_{\omega zy} & 0 \end{pmatrix}$ – the matrix of the error misalignment of FOG sensitivity axes;

$\boldsymbol{\omega}(t) = (\omega_x(t); \omega_y(t); \omega_z(t))^T$ – the vector of true values of angular velocity; $\boldsymbol{\xi_\omega}(t) = (\xi_{\omega x}(t); \xi_{\omega y}(t); \xi_{\omega z}(t))^T$ – the vector of measurement noise; $\boldsymbol{\Lambda}(t) = (\lambda_0(t); \lambda_1(t); \lambda_2(t); \lambda_3(t))^T$ – the quaternion of true orientation satellite; $\boldsymbol{\delta\Psi_\Lambda} = (\delta\Psi_{\Lambda 0}; \delta\Psi_{\Lambda x}; \delta\Psi_{\Lambda y}; \delta\Psi_{\Lambda z})^T$, $\boldsymbol{\delta\Xi} = (\delta\Xi_0; \delta\Xi_x; \delta\Xi_y; \delta\Xi_z)^T$ – deterministic and random components of the quaternion of orientation error.

In general, a mathematical model of the satellite can be described by system of differential equations [7, 15]:

$$\begin{cases} \dot{\mathbf{\Lambda}}(t) = 0.5\mathbf{\Lambda}(t) \circ \boldsymbol{\omega}(t); \\ \mathbf{I}\dot{\boldsymbol{\omega}}(t) + (\boldsymbol{\omega}(t) \times \mathbf{I}\boldsymbol{\omega}(t)) + \mathbf{L}\ddot{\mathbf{x}}(t) = \mathbf{M}(t); \\ \ddot{\mathbf{x}}(t) + \mathbf{K}\dot{\mathbf{x}}(t) + \mathbf{C}\mathbf{x}(t) = \mathbf{Q}\dot{\boldsymbol{\omega}}(t); \\ \dot{\boldsymbol{\theta}}(t) = \boldsymbol{\omega}(t), \end{cases}$$

where $\mathbf{\Lambda}(t)$ – the quaternion of satellite orientation; $\mathbf{I}$ – the matrix of inertia moments of satellite relative to coordinate system when elastic elements are undeformed; $\boldsymbol{\omega}(t) = (\omega_x(t); \omega_y(t); \omega_z(t))^T$ – the angular velocity rotation vector of satellite projected on the same axis; $\mathbf{M}(t) = (M_x(t); \quad M_y(t); \quad M_z(t))^T$ – the vector of torque control; $\mathbf{L}$ – the matrix of influence of elastic elements (solar panels, antennas, bars and other design elements) to the motion of hard core; $\mathbf{Q}$ – the matrix of influence of motion of the hard core on dynamics of elastic elements; $\mathbf{x}(t), \dot{\mathbf{x}}(t)$ – the vector of generalized coordinates and its derivative, which describe the vibrations of elastic elements; $\mathbf{K}$ – the matrix of damping coefficients; $\mathbf{C}$ – the matrix of squares of natural frequencies of elastic elements; $\boldsymbol{\theta}(t)$ – the vector of apparent angle of satellite rotation.

Calibration of zero bias and scale factors. Evaluation of zero bias of inertial unit is realized by means of a stationary observer of Luenberger type with extended state vector in accordance with the system [15, 16]:

$$\begin{cases} \dot{\mathbf{\Lambda}}(t) = 0.5\mathbf{\Lambda}(t) \circ (\boldsymbol{\omega}^*(t) + \mathbf{K}_B \cdot \text{vect}(\Delta\mathbf{\Lambda}(t)) - \Delta\boldsymbol{\omega}(t)); \\ \Delta\dot{\boldsymbol{\omega}}(t) = -\mathbf{K}_U \cdot \text{vect}(\Delta\mathbf{\Lambda}(t)), \end{cases} \quad (6)$$

where $\boldsymbol{\omega}^*(t)$ – the angular velocity obtained by FOG measurements (4); $\Delta\boldsymbol{\omega}(t)$ – the evaluation of the angular velocity of ICS drift; $\mathbf{K}_U, \mathbf{K}_B$ – the column matrices of filter coefficients; $\Delta\mathbf{\Lambda}(t)$ – the quaternion of mismatch $\Delta\mathbf{\Lambda}(t) = \mathbf{\Lambda}^{-1}(t) \circ \mathbf{\Lambda}^*(t)$; $\mathbf{\Lambda}^*$ – the quaternion of orientation which obtained by star tracker readings (5).

This algorithm was effective and was able to identify accurately the error of zero signal under the influence of other errors as in the background, and in special modes. Numerical values of the filter coefficients (6) may be selected from a given performance and from desired steady-state error of evaluation.

The following values of the FOG measurement errors are used for mathematical modeling:

$$\delta\mathbf{K}_\omega = \begin{pmatrix} -0.005 & 0 & 0 \\ 0 & -0.002 & 0 \\ 0 & 0 & -0.004 \end{pmatrix}; \quad \delta\mathbf{\Psi}_\omega = \begin{pmatrix} 0 & 2.5 \cdot 10^{-5} & -3 \cdot 10^{-5} \\ -2.5 \cdot 10^{-5} & 0 & -2 \cdot 10^{-5} \\ 3 \cdot 10^{-5} & 2 \cdot 10^{-5} & 0 \end{pmatrix};$$

$$\Delta\boldsymbol{\omega} = (1 \cdot 10^{-4}; 2 \cdot 10^{-4}; -1.5 \cdot 10^{-4})^T, \text{ rad/s}.$$

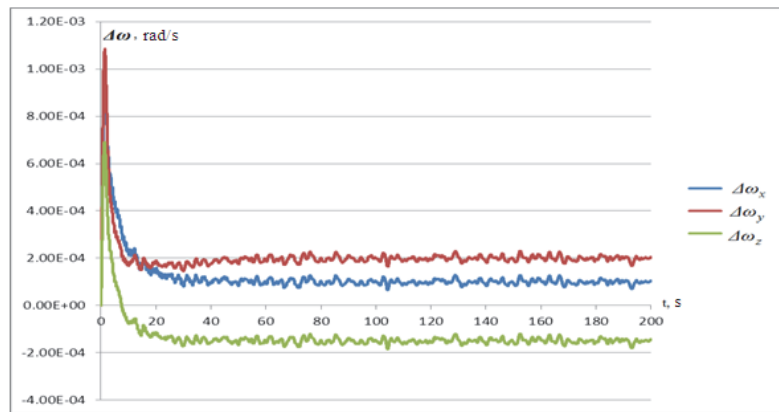The results of simulation are presented in Fig. 7.

Fig. 7. The evaluation of zero bias

Fig. 7 shows that zero bias may be identified with high accuracy and separately from other components of the error. It should be noted that for the above process the final value of zero bias must be received by averaging it on a steady plot of evaluation.

An algorithm of identification of zero signal error can also be built on the basis of calculating the orientation error accumulated during the operation of the system on the gyroscopes memory.

The following procedure applies to determine of the scale factor error. The satellite is aimed at a known point (this can be any object whose coordinates are known with great precision and which not change its position during the experiment, such as a star) with a great accuracy. The adjustment of orientation quaternion Λ is produced by the indications of star tracker. A angular maneuver of satellite is carried out around the axis orthogonal to the sighting axis of the star on a certain angle, e.g. 360°. The difference between the indications of AIS and FOG enables us to determine the scale factors errors.
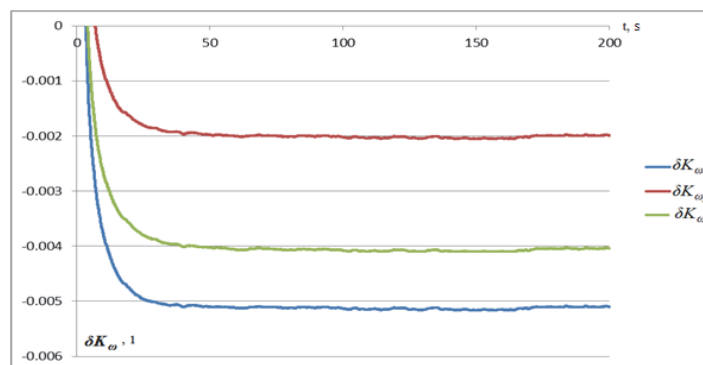
The simulation results are shown in Fig. 8.

Fig. 8. Evaluation of the scale factors errors

Determination of error misalignment of sensitivity axes of IMU and star tracker. The approach has been borrowed from [13, 14], discussed in more detail and presented in the form of the algorithm in [17].

The developed algorithm is based on estimates of projections of angular velocity of the satellite derived from measurements of FOG and star tracker. Matrix of mismatch axes of the ICS of FOG and star tracker is calculated from the interconnection of equations of angular velocity by recursive least squares method. This approach is advisable to apply after calibration of zero bias and scaling factors of FOG by the methods described above.

The results of mathematical modeling revealed that the relative orientation of the axes of star tracker ICS and sensitivity axes of FOG can be determined with an accuracy of about 20″.

The above methods allow us to identify the error scale factor, zero bias of FOG and misalignment of IMU ICS and star tracker ICS with high accuracy in the process of operating the satellite in orbit.

The achieved accuracy characteristics

Validation of the developed thermo-compensational models, re-testing based on the results of IMU ground calibration, and mathematical modeling of the orbital calibration allowed the estimates of accuracy characteristics of the developed device.

We give the accuracy characteristics of sensitive elements – OIUS-501-type FOG before and after the ground calibration and temperature compensation as a part of IMU.

The accuracy characteristics of FOG before / after calibration as a part of IMU

Zero signal, °/h:
   - systematic ………………………..………………………..……..… ±1.0 / -
   - random (3σ) …………..…………………………….....……….. ±0.3 / ±0.05
Spectral density of noise power, °/√h ……………………...……………… 0.005
Scale factor error, %……………………………....................………..… ±0.1 / ±0.002
FOG SA orientation error relative
to the plane of mating place, ang. s …………………………………....…. ±300 / -
FOG SA orientation error in IMU ICS, ang. s ………………....... ±306 / ±20 (total)

The task of eliminating the effect of instrumental and computational drifts for strapdown inertial system for space purposes is solved by celestial measurements of star tracker. Therefore, this system was named as strapdown stellar-inertial system (SSIS).

The forecasted accuracy and basic specifications of SSIS are listed below.

The accuracy characteristics of SSIS after ground / orbital calibration

The error in determining the angular velocity of the SSIS ICS, °/h ..... ±0.12 / ±0.10
Rate of drift of orientation quaternion of SSIS ICS, °/h ……......... ±0.21 / ±0.17
The error in determining orientation
of the star tracker ICS in 2ECS, ang. s ……………………...…..…...… ±22
The error in determining orientation
of the SSIS ICS in 2ECS, ang. s ……………………………...…..….. ±67 / ±30

To calculate of errors in determining orientation the characteristics of star tracker developed by enterprise Arsenal (Kiev) were used.

The basic technical characteristics of SSIS

Appointment ……………………………………………..…...…… spacecraft
Type of angular velocity sensors .... OIUS-501-type FOG
Measuring range of angular velocity,°/s ……………………...….…………. ±10
Quantity of FOGs …………………………………….……………..….….. 4
Data interface …………………………………….…….…………….. RS-422/485
Output information update period, ms …………………….……………...... 5
Time of operational readiness, s …………………………………………..… 3
Time of accuracy readiness, min ……………….……………….………...... 30
Power supply voltage, V …………….…………...…………………….…... 24…34
Power consumption with three FOGs, W …………………….…….…… 12.5
Guaranteed useful life, h …………….………………………………….… 65000
Temperature range, °C …………….……………………….......………. +10…+40
Mass, kg ………………………….………………………………………..... 5.5
Overall dimensions, mm ……………….…………………….………… 210×210×205

Strapdown inertial system (SIS) for rocket purposes integrates with hardware of consumer of satellite navigation system GPS/GLONASS.

Determining the accuracy characteristics of SIS is under consideration. The forecasted basic specifications of SIS are listed below.

The main technical characteristics of SIS

Appointment .... launch vehicles
Type of angular velocity sensors .... OIUS-501-type FOG
Type of accelerometer …………………………………………… pendulum AK-30
Measuring range of the angular velocity, °/s ....….. ±100
Measuring range of linear acceleration , m/s^2 .... ±85
Quantity of FOGs 3
Quantity of accelerometers 3
Data interface ……………………………………………...…...... RS-422/485
Output information update period, ms 1.25
Time of operational readiness, s ....….. 3
Time of accuracy readiness, min 30
Power supply voltage, V .... 24 ... 34
Power consumption, W 15.0
Guaranteed useful life, h 3000
Temperature range, °C .... -40 ... +50
Mass, kg 5.3
Overall dimensions, mm .... 205×205×160

Conclusions

The paper shows that the problem of creating a high-precision strapdown inertial system based on medium-accuracy fiber-optic gyroscopes by using the proposed methodology is feasible, which is the main result of the research.

The strapdown stella-inertial system being developed is planned to be tested as a "passenger" of the control system aboard a small satellite of the Ukrainian Mikrosat remote sensing system in 2015.

References

1. **Peshekhonov V.G.** Gyroscopic Navigation Systems: Current Status and Prospects // Gyroscopy and Navigation, vol. 2, No. 3, 2011, pp. 111-118.
2. **Zlatkin Yu.M., Oleynik S.V., Kuznyetsov Yu.A., Uspenskiy V.B., Bagmut I.A**. Technology and results of tests of the strap-down star-inertial unit for control systems of spacecrafts // 19th Saint Petersburg International Conference on Integrated Navigation Systems. Proceedings. – Saint Petersburg: CSRI "Elektropribor", 2012, pp. 238-241.
3. **Korkishko Ju.N., Fedorov V.A., Prilutskii V.E., Ponomarev V.G., Morev I.V., Skripnikov S.F., Khmelevskaya M.I., Buravlev A.S., Kostritskii S.M., Zuev A.I., Varnakov V.K.** Strapdown inertial navigation system based on fiber-optic gyroscopes // Sb. trudov XX Sankt-Peterburgskoi mezhdunarodnoi konferencii po integrirovannym navigatsionnym sistemam. Sankt-Peterburg, CNII «Elektropribor», 2013, pp. 75-82.
4. **Buravlev A.S., Egorov D.A., Lisin L.G**. Fiber optic gyroscopes under constant magnetic field // Giroskopija i navigatsija. – № 3 (62), 2008, pp. 59-63.
5. **Zlatkin Ju.M., Olejnik S.V., Kuznetsov Ju.A., Uspenskii V.B**. Results of the study of the effect of the Earth's magnetic field to the measurement error of fiber-optic gyroscope // Nauchno-tekhn. sb. «Kosmicheskaja tekhnika. Raketnoe vooruzhenie». – Dnepropetrovsk: GP «KB «Juzhnoe», 2011, pp. 122-132.
6. **Chumachenko A.V., Firsov S.N., Kuznetsov Ju.A., Uspenskii V.B., Golub E.Ju.** Methods of determining and test results of the effect of the Earth's magnetic field to operation of fiber optic gyroscopes // Radioelektronni i komp'juterni sistemi, 2012, № 2 (54), pp. 66-71.
7. **Alekseev K.B., Bebenin G.G.** Upravlenie kosmicheskimi letatel'nymi apparatami (Control of a spacecraft). – M.: Mashinostroenie, 1974. – 340 pp.
8. **Sheremet'ev A.G.** Volokonnyi opticheskii giroskop (Fiber-optic gyroscope). – M.: Radio i svjaz', – 1987. – 152 pp.
9. **Kuznetsov Ju.A., Olejnik S.V., Uspenskii V.B., Hats'ko N.E.** Developing a model of drift of OIUS 501-type FOG under temperature sensor changes // Matematicheskie metody v tehnike i tehnologijah – MMTT-25: sb. trudov XXV Mezhdunar. nauch. konf.: v 10 t. – Vol. 6. – Section 10. – Volgograd: Volgogr. gos. tekhn. un-t, 2012; – Khar'kov: Natsion. tekhn. un-t «HPI», 2012, pp. 82-84.
10. **Statisticheskie metody** v inzhenernyh issledovanijah: Ucheb. posobie (Statistical methods in engineering studies: Studies allowance) / Borodjuk V.P. i dr.; Pod red. G.K.Kruga. – M.: Vyssh. shkola, 1983. – 216 pp.
11. **Emel'jancev G.I., Nesenjuk L.P., Blazhnov B.A., Stepanov A.P.** On peculiarities of calibration of strapdown inertial module on fiber-optic gyroscopes as a part of an integrated system during orbital flight of spacecraft // Giroskopija i navigacija, 2008, № 2 (61), pp. 39-53.
12. **Lebedev D.V., Tkachenko A.I.** Calibration of information-measuring complex of spacecraft, designed to capture the earth's surface // Problemy upravlenija i informatiki, 2004, № 1, pp. 101-120.
13. **Somov E.I., Butyrin S.A.** Digital signal processing, calibration and adjustment of platform inertial system for determining orientation of maneuvering spacecraft // Sb. materialov XVII Sankt-Peterburgskoi Mezhdunarodnoi konferencii po integrirovannym navigacionnym sistemam. Sankt-Peterburg, CNII «Elektropribor», 2010, pp. 75-77.
14. **Somov E.I., Butyrin S.A., Skirmunt V.K.** Flight geometric calibration system of Space Telescope and star sensors // Sb. materialov XV Sankt-Peterburgskoi Mezhdunarodnoi konferencii po integrirovannym navigacionnym sistemam. Sankt-Peterburg, CNII «Elektropribor», 2008, pp. 130-135.
15. **Branec V.N., Shmyglevskii I.P.** Primenenie kvaternionov v zadachah orientacii tverdogo tela (Application of quaternions in problems of orientation of a rigid body). – M.: Nauka, 1973. – 320 pp.
16. **Kuzovkov N.T.** Modal'noe upravlenie i nabljudajushhie ustrojstva (Modal control and observing devices). – M.: Mashinostroenie, 1976. – 270 pp.
17. **Kuznetsov Ju.A., Gudzenko A.V.** Development of algorithms for determining the error of mutual installing of ARS and ST control system of spacecraft // Matematicheskie metody v tehnike i tehnologijah – MMTT-25: sb. trudov XXV Mezhdunar. nauch. konf.: v 10 t. – Vol. 6. – Section 10. – Volgograd: Volgogr. gos. tehn. un-t, 2012; – Khar'kov: Natsion. tekhn. un-t «HPI», 2012, pp. 77-79.